AIP | Applied Physics Letters

Nonlinear electron dynamics of gold ultrathin films induced by intense terahertz waves

Yasuo Minami, Jun Takeda, Thang Duy Dao, Tadaaki Nagao, Masahiro Kitajima, and Ikufumi Katayama

Citation: Applied Physics Letters **105**, 241107 (2014); doi: 10.1063/1.4904883
View online: http://dx.doi.org/10.1063/1.4904883
View Table of Contents: http://scitation.aip.org/content/aip/journal/apl/105/24?ver=pdfcov
Published by the AIP Publishing

Nonlinear electron dynamics of gold ultrathin films induced by intense terahertz waves

Yasuo Minami,[1,a)] Jun Takeda,[1] Thang Duy Dao,[2,3] Tadaaki Nagao,[2,3] Masahiro Kitajima,[1,2,3,4,5] and Ikufumi Katayama[1]
[1]*Department of Physics, Graduate School of Engineering, Yokohama National University, Yokohama 240-8501, Japan*
[2]*International Center for Materials Nanoarchitectonics, National Institute for Materials Science, Tsukuba 305-0044, Japan*
[3]*JST-CREST, Kawaguchi 332-0012, Japan*
[4]*LxRay Co. Ltd., Nishinomiya 663-8172, Japan*
[5]*Department of Applied Physics, National Defense Academy, Yokosuka 239-8686, Japan*

(Received 24 August 2014; accepted 10 December 2014; published online 17 December 2014)

Linear and nonlinear electron dynamics of polycrystalline gold (Au) ultrathin films with thicknesses ranging from 1.4 to 5.8 nm were investigated via transmittance terahertz (THz) spectroscopy with intense electric field transients. We prepared ultrathin films with low surface roughness formed on a Si–(7×7) reconstructed surface, leading to the observation of monotonic decrease in THz transmittance with respect to film thickness. Furthermore, at all tested thicknesses, the transmittance decreased nonlinearly by 10%–30% with the application if high-intensity THz electric fields. Based on a Drude-model analysis, we found a significant decrease in the damping constant induced by the THz electric field, indicating that electrons are driven beyond the polycrystalline grain boundaries in Au thin films, and consequently leading to the suppression of the electron–boundary scattering rate. © *2014 AIP Publishing LLC*. [http://dx.doi.org/10.1063/1.4904883]

Gold (Au) has been extensively studied in the fields of microelectronics[1–6] and bio-sensing[7–13] because of its high conductivity and chemical stability. In the fabrication of nanoscale plasmonic devices, Au nanostructures have been widely used to enhance the local electric field. This not only helps in detecting linear phenomena sensitively but also drives nonlinear phenomena, including phase transitions.[14] Therefore, understanding the linear and nonlinear electron dynamics of Au nanostructures is of particular importance. Linear electron dynamics in granular Au films has been extensively examined in terahertz (THz) regions.[15–20] For example, the effective sheet conductivity of Au thin films dramatically decreases for thicknesses below 2 nm.[17] This implies that the morphology of Au nanostructures plays an important role on their electromagnetic properties. Although determining the intrinsic electron dynamics of crystalline and non-porous Au is an essential prerequisite to discussing how the morphology of Au nanostructures affects their electromagnetic properties, only a few studies have explored the THz conductivity in non-porous Au films with thicknesses above 4–20 nm;[21,22] the thicker film samples make difficult to directly measure the THz transmittance spectra. In the present study, we fabricated high-quality smooth, flat, and non-porous Au-polycrystalline ultrathin films of varying thicknesses in a range of 1.4–5.8 nm. We then investigated the linear and nonlinear electron dynamics of these films using transmittance THz spectroscopy with intense electric fields.[23–25] Based on a Drude-model analysis, we clarified the nonlinear electron dynamics in Au ultrathin films, whose characteristics may be useful in designing nonlinear plasmonic devices.

The polycrystalline Au ultrathin films were evaporated on a high-resistivity, flashed, and atomically flat Si(111)–7×7 reconstructed surface by molecular beam epitaxy (MBE) in an ultrahigh vacuum chamber ($<10^{-7}$ Pa) at room temperature with the evaporation rate of about 1 Å/min. We obtained several Au ultrathin films with different thicknesses of 1.4, 1.6, 1.9, 3.0, 4.8, and 5.8 nm, whose crystallographic structure was verified using reflection high-energy electron diffraction (RHEED). The thickness was monitored by a frequency of the quartz oscillator (SQM-160, Inficon). To obtain the properly smooth, flat, and non-porous polycrystalline specimen, we prepared a substrate with clean surface using the similar method reported previously.[26] The desired quality of surface morphology was confirmed using a scanning electron microscope (SEM). Figure 1(a) shows SEM images of the specimens with thicknesses of 1.9 nm (top) and 5.8 nm (bottom). Judging from the gradation of the SEM images, the films had an area of $>2 \times 2\,\text{mm}^2$, which was fully coated by polycrystalline ultrathin Au. We also found that the polycrystal grain size was typically 3–5 nm in diameter for all specimens, which is smaller than the mean free path of electrons in single-crystal Au (~25 nm).[18]

A Ti:Sapphire amplifier system (repetition rate: 1 kHz, pulse duration: 130 fs, center wavelength: 800 nm, and pulse energy: ~1.9 mJ/pulse) was employed to generate intense THz waves (maximum THz field: ~280 kV/cm $\equiv E_0$). The THz fields were produced by irradiating a $LiNbO_3$ prism with a pulse-front-tilted laser using a Cherenkov-type phase-matching process.[27] The generated THz waves were incident on the specimen with varying intensity, tuned by a set of two-wire grid polarizers placed in front of the specimen. Then, the transmitted THz waves were forwarded to a 0.4-mm-thick GaP crystal using off-axis parabolic mirrors to

[a)]Email: minamiyasuo@ynu.ac.jp

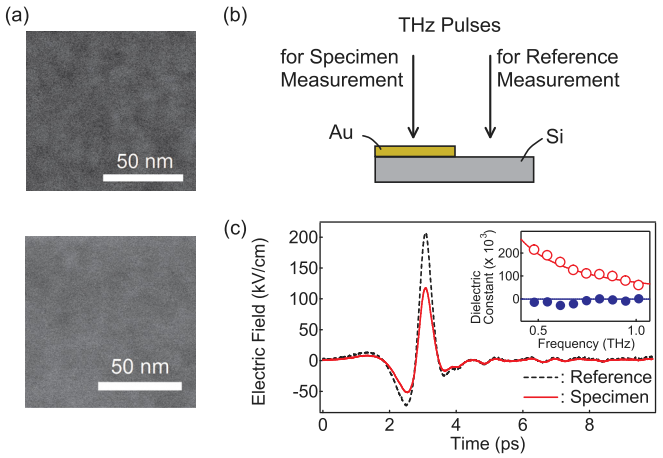

FIG. 1. (a) SEM images of the specimens with thicknesses of 1.9 nm (top) and 5.8 nm (bottom). (b) Side view of the specimen placement used for measuring signal- and reference-THz transmittance. (c) Typical transient THz waveforms for the reference (dashed curve) and the signal (solid curve) with the 1.9-nm-thick Au film. The inset shows the complex permittivity spectrum of the 1.9-nm-thick Au film. The real and imaginary parts are shown by closed and open circles. The solid curves come from the Drude fits.

observe the electric field transient by electro-optic (EO) sampling. Finally, the transmittance THz spectrum was obtained by normalizing the transmitted waveform from the Au ultrathin film on Si substrate with that of a plain Si substrate (reference waveform), as shown by Figs. 1(b) and 1(c). Application of transmittance THz-time-domain spectroscopy to metal thin films allows for direct observation of electron dynamics in the specimen, since the complex conductivity spectra are obtained directly from the complex permittivities, which are analyzed with the Drude model as shown by the inset of Fig. 1(c). Owing to this merit, we can quantitatively evaluate the linear and nonlinear dynamics of electrons in Au films.

Figure 2(a) shows the film-thickness dependence of transmittance averaged over 0.4–1.1 THz. The observed transmittances are much smaller than those reported in Ref. 18 (~100%) which employed the sputter deposition method, and therefore, resulted in a more granular structure and substantial surface roughness compared to the specimens produced by MBE. Thus, the discrepancy in transmittance most likely comes from the different morphology and indicates a relatively strong THz-range absorption in our specimens. Here, we emphasize that transmittance decreases monotonically with thickness, indicating that we may observe the intrinsic complex dielectric constants of Au, or, in other words, that the elementary electromagnetic properties of Au ultrathin films were made calculable by our experiment. The more interesting property observed is the maximum electric-field dependence of the transmittance, which is shown in Fig. 2(b). To highlight the change in transmittance, the values are normalized with the weakest electric field as unity. The normalized transmittance becomes 10%–30% lower with increasing electric-field, which is evidence of the nonlinear electron dynamics in Au. This nonlinear behavior is almost entirely independent of film thickness, since our specimens are homogeneous and polycrystalline.

A Drude-model analysis was carried out to evaluate the complex dielectric constant of the specimens in the THz range.

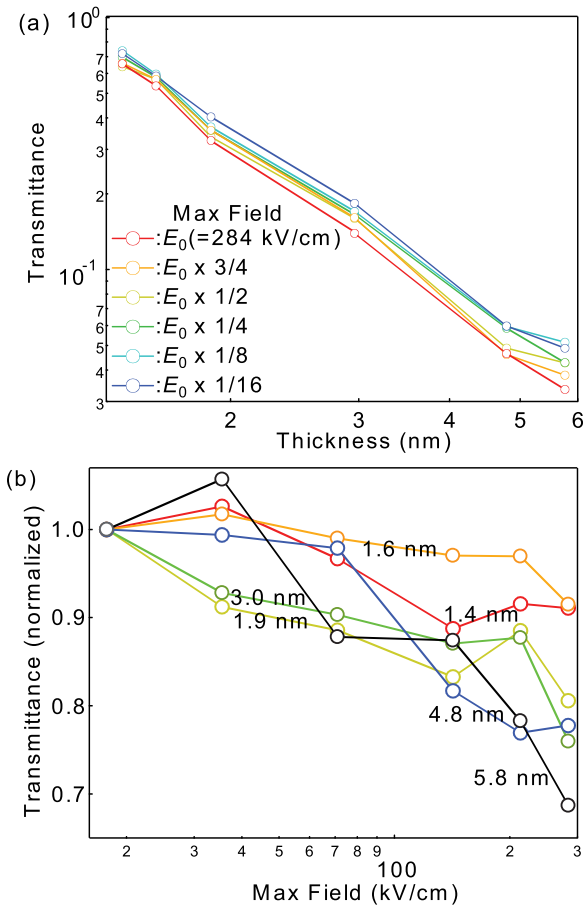

FIG. 2. (a) Averaged THz transmittance as a function of Au-film thickness with several THz intensities. E_0 denotes a maximum electric field (284 kV/cm). (b) The normalized transmittance as a function of maximum electric-field strength for various film thicknesses. The transmittance is normalized by the weakest electric field ($E_0/16$).

The relationship between the observed complex transmittance $\tilde{T}$ and the dielectric constant at each angular frequency ω, under the thin-film approximation, is expressed as[28]

$$\tilde{T} = \frac{(n_{\mathrm{Si}} + 1)}{n_{\mathrm{Si}} + 1 - i\omega\tilde{\varepsilon}d/c}, \tag{1}$$

where $\tilde{\varepsilon}$ illustrates the Drude-type dielectric dispersion: $\tilde{\varepsilon} = \varepsilon_\infty - \frac{\omega_p^2}{\omega(\omega+i\gamma)}$. Here, ε_∞ (≈ 1) is the dielectric constant at the high-frequency limit, ω_p is the plasma frequency of free electrons, γ is the damping constant, c is the speed of light, n_{Si} is the refractive index of the Si substrate, and d is the thickness of the specimen. The damping constant γ describes the rate of electron–electron scattering and/or electron–boundary scattering. According to the above equations, the transmittance becomes lower with either increased plasma frequency or a reduced damping constant. The plasma frequency is defined as

$$\omega_p = \sqrt{\frac{ne^2}{\varepsilon_0 m^*}}, \tag{2}$$

where n is the electron density, m^* is the electron effective mass, e is the elementary charge, and ε_0 is the dielectric constant in vacuum. Figure 3 shows the Au-thickness dependences of the estimated plasma frequency (open circles) and of the

estimated damping constant (solid circles) under the weakest electric field ($E_0/16$). Except for the extremely thin specimens (<2 nm), both the plasma frequency and damping constant are practically independent of the thickness, with estimated values of 13×10^{15} rad/s and $300 \times 10^{12}\,s^{-1}$, respectively. The estimated plasma frequency is slightly smaller than that of the bulk specimen (14×10^{15} rad/s), whereas the damping constant is larger than that of the bulk specimen ($38 \times 10^{12}\,s^{-1}$),[29] however slightly smaller than that of the porous specimen ($330 \times 10^{12}\,s^{-1}$).[22] The slight decrease of the estimated plasma frequency may be attributable to carrier trapping due to the presence of grain boundaries. Since we use polycrystalline Au thin films in this study, the damping constant is expected to be larger than that of single-crystalline Au, while smaller than that of granular or typical porous specimens, depending on the abundance of grain boundaries. In specimens thinner than 2 nm, the plasma frequency decreases and the damping constant increases with reduced thickness, as shown in Fig. 3, which is probably due to the effects of surface roughness.

The plasma frequency and damping constant as functions of the maximum electric field with various film thicknesses are shown in Figs. 4(a) and 4(b), respectively. The plasma frequency is slightly enhanced (~5%) by the intense THz field, and the value approaches that of the bulk specimen (14×10^{15} rad/s), while showing negligible thickness dependence, as expected. However, the damping constant significantly decreases (10%–30%), while remaining independent of the film thickness. The decrease of the damping constant implies the increase of the conductivity in polycrystalline Au thin films, since a conductance σ is expressed as $\sigma = ne^2/\gamma m^*$. It is known that the conductance of metal thin films with many small discrete islands becomes higher as temperature increases,[30] as a result of the increase of the tunneling rate between islands; the temperature rise of 70 K leads to the 25% increase of the conductance or the 20% decrease of the damping constant in Ref. 30. Assuming that the same situation can be applied to polycrystalline Au thin films, we estimated the temperature rise induced by the applied THz field. The lattice temperature rise for the 4.8-nm-thick film by 280 kV/cm-THz-field illumination is negligible for the increase of the conductance in the time region. In contrast, the mean free path $l\,(=v_F/\gamma)$ of the 4.8-nm-thick film was estimated to be 6.4 nm using a Fermi velocity (v_F) of 1.4×10^6 m/s and the

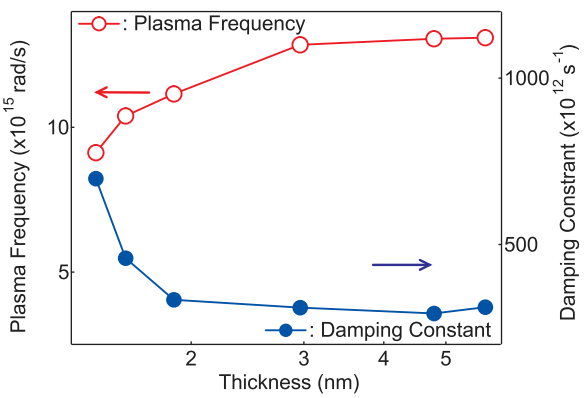

FIG. 3. Plasma frequency (open circles) and damping constant (solid circles) in the $E_0/16$ field obtained by the Drude analysis as a function of film thickness.

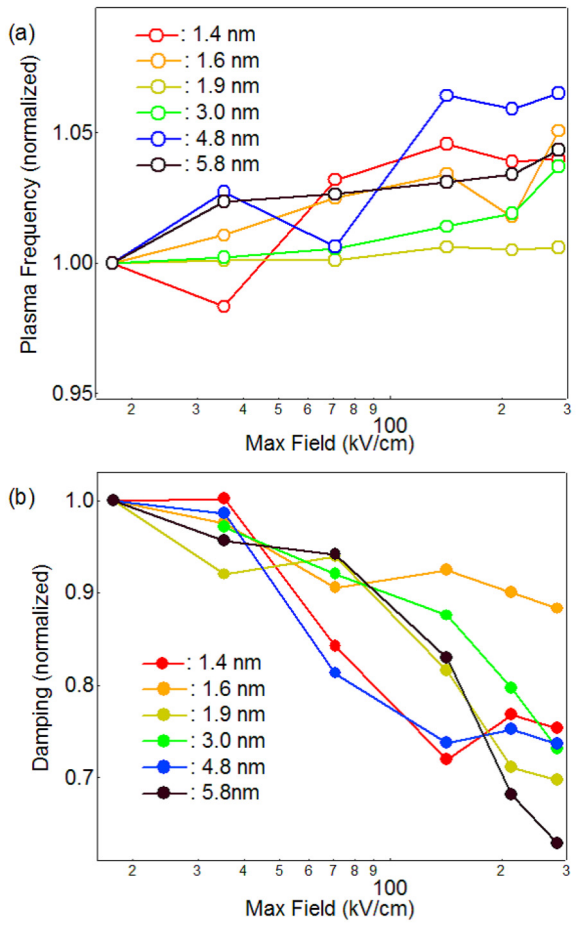

FIG. 4. (a) The plasma frequency and (b) the damping constant of the Au film vs. the maximum electric field, normalized as by the weakest electric field ($E_0/16$). The standard deviation of the normalized plasma frequency and of the normalized damping constant is 0.022 and 0.13, respectively.

observed damping constant of $220 \times 10^{12}\,s^{-1}$ induced by the applied THz field of 280 kV/cm, whose value is larger than the typical grain size of 3–5 nm. The larger mean free path over the grain size most likely results from the decrease of the electron–boundary scattering rate; the intense THz electric field can drive free electrons beyond the grain boundaries without lattice heating, leading to the suppression of the electron–boundary scattering rate. The reduced damping constant is the primary factor in the nonlinear-transmittance response in polycrystalline Au ultrathin films, where the intense THz field significantly reduces the boundary effect.

In summary, we have measured a nonlinear, 10%–30% reduction in the transmittance of Au ultrathin films in the THz region, with thicknesses ranging from 1.4 to 5.8 nm, using intense electric fields. Thus, by using non-porous polycrystalline Au, we were able to evaluate the inherent nonlinear electron dynamics of Au. A Drude analysis revealed a considerable reduction in the damping constant, indicating that such intense, high electric fields drive electrons beyond the polycrystalline grain boundaries in Au thin films, leading to the suppression of the electron–boundary scattering rate. Our findings suggest that the nonlinear electron transport induced by such fields should be taken into account in the analysis of electromagnetic properties of metallic nanostructures, where electric-field enhancement occurs readily.

This work was supported in part by the Grants-in-Aid for Scientific Research (KAKENHI, Nos. 23104713, 23241034, 25104712, and 25800177) from the Japan Society for the Promotion of Science (JSPS).

[1]P. Bon, N. Belaid, D. Lagrange, C. Bergaud, H. Rigneault, S. Monneret, and G. Baffou, Appl. Phys. Lett. **102**, 244103 (2013).
[2]A. Thran, T. Strunskus, V. Zaporojtchenko, and F. Faupel, Appl. Phys. Lett. **81**, 244 (2002).
[3]E. Zahidi, H. Oudghiri-Hassani, and P. H. McBreen, Nature **409**, 1023 (2001).
[4]H. Y. Fan, Y. F. Lu, A. Stump, S. T. Reed, T. Baer, R. Schunk, V. Perez-Luna, G. P. López, and C. J. Brinker, Nature **405**, 56 (2000).
[5]A. I. Yanson, G. R. Bollinger, H. E. van den Brom, N. Agraït, and J. M. van Ruitenbeek, Nature **395**, 783 (1998).
[6]A. Hellemans, Science **279**, 484 (1998).
[7]C. V. Hoang, M. Oyama, O. Saito, M. Aono, and T. Nagao, Sci. Rep. **3**, 1175 (2013).
[8]F. Neubrech, D. Weber, D. Enders, T. Nagao, and A. Pucci, J. Phys. Chem. C **114**, 7299 (2010).
[9]A. I. Aristov, U. Zywietz, A. B. Evlyukhin, C. Reinhardt, B. N. Chichkov, and A. V. Kabashin, Appl. Phys. Lett. **104**, 071101 (2014).
[10]C. Huang, J. Ye, S. Wang, T. Stakenborg, and L. Lagae, Appl. Phys. Lett. **100**, 173114 (2012).
[11]M. A. Santiago-Cordoba, S. V. Boriskina, F. Vollmer, and M. C. Demirel, Appl. Phys. Lett. **99**, 073701 (2011).
[12]Y. L. Liu and K. W. Sun, Appl. Phys. Lett. **98**, 153702 (2011).
[13]A. Kiristopuryan, Y. Ekinci, R. Giannini, P. K. Sahoo, G. Gorodyska, and J. F. Löffler, Appl. Phys. Lett. **95**, 231903 (2009).
[14]M. Liu, H. Y. Hwang, H. Tao, A. C. Strikwerda, K. Fan, G. R. Keiser, A. J. Sternbach, K. G. West, S. Kittiwatanakul, J. Lu, S. A. Wolf, F. G. Omenetto, X. Zhang, K. A. Nelson, and R. D. Averitt, Nature **487**, 345 (2012).
[15]S. Xia, D. Yang, T. Li, X. Liu, and J. Wang, Opt. Lett. **39**, 1270 (2014).
[16]A. Pimenov and A. Loidl, Phys. Rev. B **74**, 193102 (2006).
[17]J. J. Tu, C. C. Homes, and M. Strongin, Phys. Rev. Lett. **90**, 017402 (2003).
[18]M. Walther, D. G. Cooke, C. Sherstan, M. Hajar, M. R. Freeman, and F. A. Hegmann, Phys. Rev. B **76**, 125408 (2007).
[19]J. Siegel, O. Lyutakov, V. Rybka, Z. Kolská, and V. Švorcík, Nanoscale Res. Lett. **6**, 96 (2011).
[20]C. A. Davis, D. R. McKenzie, and R. C. McPhedran, Opt. Commun. **85**, 70 (1991).
[21]N. Laman and D. Grischkowsky, Appl. Phys. Lett. **93**, 051105 (2008).
[22]T. Brandt, M. Hövel, B. Gompf, and M. Dressel, Phys. Rev. B **78**, 205409 (2008).
[23]Y. Minami, T. Kurihara, K. Yamaguchi, M. Nakajima, and T. Suemoto, Appl. Phys. Lett. **102**, 151106 (2013).
[24]Y. Minami, T. Kurihara, K. Yamaguchi, M. Nakajima, and T. Suemoto, Appl. Phys. Lett. **102**, 041105 (2013).
[25]H. Hirori, A. Doi, F. Blanchard, and K. Tanaka, Appl. Phys. Lett. **98**, 091106 (2011).
[26]T. Nagao, S. Hasegawa, K. Tsuchie, S. Ino, C. Voges, G. Klos, H. Pfnür, and M. Henzler, Phys. Rev. B **57**, 10100 (1988).
[27]J. Hebling, G. Almási, and I. Kozma, Opt. Express **10**, 1161 (2002).
[28]K. Yokota, J. Takeda, C. Dang, G. Han, D. N. McCarthy, T. Nagao, S. Hishita, M. Kitajima, and I. Katayama, Appl. Phys. Lett. **100**, 251605 (2012).
[29]M. A. Ordal, L. L. Long, R. J. Bell, S. E. Bell, R. R. Bell, R. W. Alexander, Jr., and C. A. Ward, Appl. Opt. **22**, 1099 (1983).
[30]C. A. Neugebauer and M. B. Webb, J. Appl. Phys. **33**, 74 (1962).